UACJ | UNIVERSIDAD AUTÓNOMA DE CIUDAD JUÁREZ

Departamento de Ingeniería Industrial y Manufactura

Instituto de Ingeniería y Tecnología

SAE Aero Design West 2018

Design Report

UACJ AERO TEAM

M.I. Geovani E. García - Faculty Advisor

M.I. Alfredo Villanueva - Program Coordinator

Dr. Abimael Jiménez - Adviser

M.I. Manuel A. Lira – Adviser

M.I. Arturo Paz – Adviser

Gustavo Fernandez Beltrán - Team Captain

Maricela Hinojo Barrios

Giezi Xitlali Chávez Serrano

Israel Sánchez Gómez

Alejandro Domínguez Márquez

Daniel Fernando Gurrola Castillo

March 2018

Cd. Juárez, Chihuahua

Contents

List of figures and tables. 3

Statement of Compliance. 4

Acronyms and Symbols 4

1. Executive Summary 5

1.1 System Overview 6

1.2 Team objectives 6

2. Schedule Summary 6

2.1 Team Organization 7

2.2 General Methodology 7

2.3 Risks consideration. 8

3 Environment Considerations 9

4. Overall Design Layout 9

4.1 Propulsion System 9

4.1.1 Engine and Propeller Selection 10

4.2 Wing Configuration and Size 11

4.2.1 Wing Surface 11

4.2.2 Airfoil Selection 12

4.2.3 Aspect Ratio 13

4.2.4 Wing Planform 13

4.3 Vehicle Configuration Selection 14

4.4 Competitive Scoring and Strategy Analysis 14

4.5 Optimization 15

5 Analysis 15

5.1 Analytical Tools (CAD, FEM, CFD, etc.) 15

5.2 Performance Analysis 15

5.2.1 Static and Dynamic Thrust 15

5.2.2 Take-off and Landing Performance 16

5.2.3 V-N diagram 17

5.2.4 Payload Prediction 17

5.2.5 Flight Performance. 18

5.2.6 Maneuver Performance 18

5.2.7 Dynamic & Static Stability 19

5.2.8 Telemetry system 21

5.3 Structural Analysis 22

5.3.1 Spar analysis 22

5.3.2 Mass Properties & Balance 23

6. Aircraft ‘s assembly. 24
7. Manufacturing process 24
8. *Cost analysis* 26
The project´s cost analysis is shown on the following table. 26
9. Conclusion. 27
2D Drawing ..... **¡Error! Marcador no definido.**
10 References 29

List of figures and tables.

Figure 1. Gantt Diagram of the Project. 7
Figure 2. Team organization 7
Figure 3. *Design Methodology in Aircraft Design Systems Engineering Approach, Mohammad.* 8
Figure 4. Comparison of different propellers 11
Figure 5 Comparison between the MH114 and MH113 airfoils: Cl vs AOA airfoil and CL/CD vs AOA of a wing with different airfoil. 13
Figure 6 Comparison between tapered and rectangular wing. 14
Figure 7 SAE scoring equation (left) and the team’s scoring assumption (right). 14
Figure 8. Efficiency comparison between last year´s model and present model. 15
Figure 9. Landing and Take-off distances. 17
Figure 10. V-N diagram. 17
Figure 11 Payload prediction graphic. 18
Figure 12 Payload prediction graphic 18
Figure 13. Load factor analysis on maneuver velocity. 19
Figure 14. Total moment coefficient around the aircraft's CG graph. 20
Figure 15. Telemetry block diagram 22
Figure 16. Shear force(top) and Bending moment diagrams (bottom) 23
Table 1. Objectives. 6
Table 2. *Parameters used to determine Reynolds number.* 9
Table 3. Engine features comparison. 10
Table 4. Wing vertical location: Advantages and disadvantages. 11
Table 5. Wing loading database. 11
Table 6. Different airfoils features. 12
Table 7. Static stability derivatives 20
Table 8. Level 1 Stability Requirements and principal mode parameters 20
Table 9. Necessary torque and summary of control surfaces dimensions 21
Table 10. Materials properties. 23
Table 11. Weight and balance analysis. 23
Image 1. OS engine mounted on the testing bench. 16
Image 2. Wing support assembly. 24
Image 3. Tail boom to fuselage and tail assembly. 24
Image 4. Airframe construction and design drawing. 25
Image 5. Ribs cutting process and wing ribs final cut. 25
Image 6. Ribs arrangement. 25
Image 7. CNC machining of wing support. 26

SAE AERO DESIGN

STATEMENT OF COMPLIANCE

Certification of Qualification

Team Name	UACJ Aero Team Advanced	Team Number	210
School	Universidad Autonoma de Ciudad Juarez		
Faculty Advisor	Geovani Esau García Sanchez		
Faculty Advisor's Email	geovani.garcia@uacj.mx		

Statement of Compliance

As Faculty Advisor, I certify that the registered team members are enrolled in collegiate courses. This team has designed, constructed and/or modified the radio controlled aircraft they will use for the SAE Aero Design 2018 competition, without direct assistance from professional engineers, R/C model experts or pilots, or related professionals.

Signature of Faculty Advisor

Team Captain Information:

Team Captain:	Gustavo Fernandez Beltran
Captain's E-mail:	gus.fdz96@gmail.com
Captain's Phone:	+ 52 044 656 324 34 56

Note:

A copy of this statement needs to be included in your Design Report as page 2 (Reference Section 4.3)

$\alpha 0$	Angle of attack at zero lift
$\alpha cl/cdmax$	Angle of attack for the maximum section lift-to-drag ratio
$\alpha cdmin$	Angle of attack for minimum section drag coefficient
$Cn\delta r$	Yawing moment coefficient with rudder deflection angle
Cyp	Side force coefficient with dimensionless rate of change of roll rate
Cyr	Side force coefficient with dimensionless rate of change of yaw rate
$Cy\beta$	Side force coefficient with sideslip angle
Cd0	Section drag coefficient at zero angle of attack
Cd_{min}	Minimum section drag coefficient
CG	Center of gravity
CL	Lift coefficient
$(Cl/Cd)_{max}$	Maximum section lift-to-drag ratio
Cl_0	Section lift coefficient at zero angle of attack
Cli	Ideal lift coefficient
Cl dcmin	Section lift coefficient for minimum section drag coefficient
Cl_{max}	Maximum lift coefficient
Clr	Rolling moment coefficient with dimensionless rate of change roll rate
$Cl\beta$	Rolling moment coefficient with dimensionless rate of change of sideslip angle
$Cl\delta a$	Rolling moment coefficient with aileron deflection angle
Cm0	Section pitching moment coefficient at zero angle off attack
Cmq	Pitching moment coefficient with dimensionless speed
$Cm\alpha$	Pitching moment coefficient due to angle of attack
$Cm\delta e$	Pitching moment coefficient with elevator deflection angle
Cnp	Yawing moment coefficient with dimensionless rate of change of roll rate
$K_{\tau 0}$	Static thrust
VH	Horizontal stabilizer volume
Vv	Vertical stabilizer volume
AR	Aspect ratio
C	Chord
CD	Drag coefficient
Di	Induced drag
Do	Parasitic drag
h	Altitude
n	Load factor
P	Pressure
Re	Reynolds number
T	Temperature
Td	Available thrust
Tr	Required thrust
V	Velocity
μ	Viscosity
ρ	Density
T_0	Temperature at sea level
τ	Torque
σmax	Maximum normal stress

1. Executive Summary

This document details the final design made by the *UACJ Aero Team* from the *Universidad Autónoma de Ciudad Juárez*, with the purpose of participating in the SAE Aerodesign 2018 Competition, in which the

methodology is explained, as well as overall design, analysis, performance, and the manufacturing process used to build this aircraft named ´´EURUS´´ (*This name will be used to future references on the report*). The main objective is to design and build an unmanned aerial vehicle capable of transporting the highest possible load as well as having a precise telemetry system for the launch of packages or dynamic loads and therefore being able to achieve excellent design performance. The current design is characterized by an optimization of the last model designed by the team. In addition, it must fulfill its mission by following the SAE design requirements and be an aircraft safe enough to operate.

1.1 System Overview

The final aircraft design consists on a monoplane and trapezoidal high-wing. The aircraft's fuselage has a truss structure with a tricycle landing gear configuration with a conventional empennage supported by a tail boom that is united to the truss structure. The propulsion system is constituted by a tractor RC engine configuration and a single 2-blade propeller. The avionics system involves a Data Acquisition System (DAS), that measures altitude and airspeed, and a First-Person View (FPV) system that allows the transmission of video in real time from the aircraft.

1.2 Team objectives

To define the objectives the team was based on the requirements established by the Society of Automotive Engineers (SAE). The following table outlines the specific goals that were defined for the development of this year's competition.

Table 1. Objectives.

	Objectives
1	Maximum payload possible
2	Precise and reliable telemetry
3	A functional releasable-payload system
4	Good lift performance
5	Good design structural
6	Improve aircraft performance

2. Schedule Summary

The team made a Gantt Diagram to manage the project, consisting in ten stages from team selection to optimization.

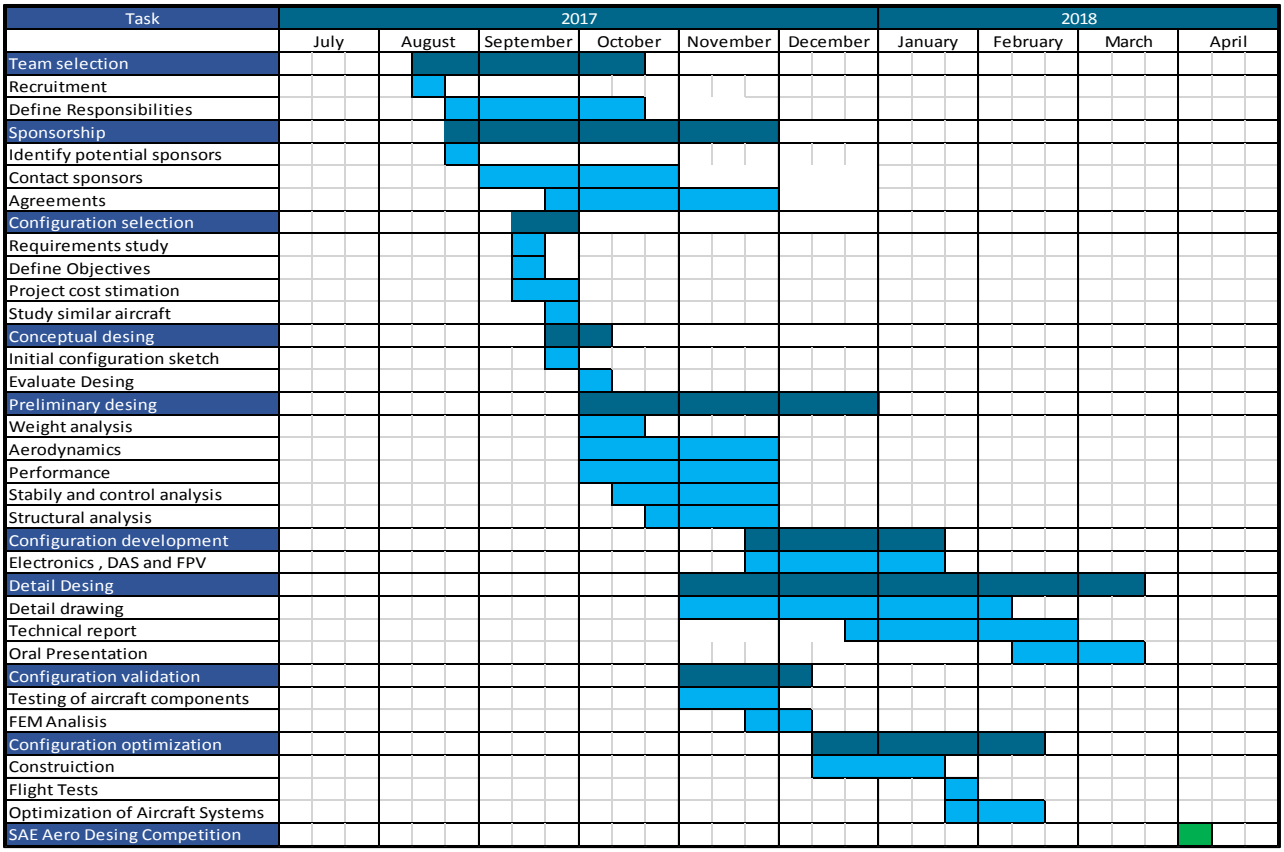

Figure 1. Gantt Diagram of the Project.

2.1 Team Organization

UACJ Aero Team is divided into five strategic groups, each one assigned to meet specific tasks on time.

F*igure 2* shows the team division.

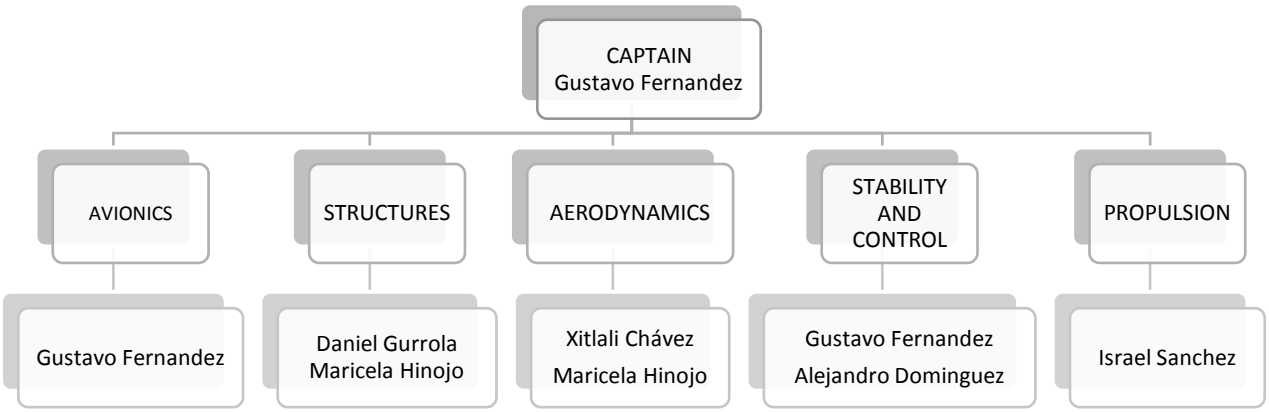

Figure 2. Team organization

2.2 General Methodology

The engineering process was based on the Mohammad book methodology and adapted by the team, as shown in the following diagram.

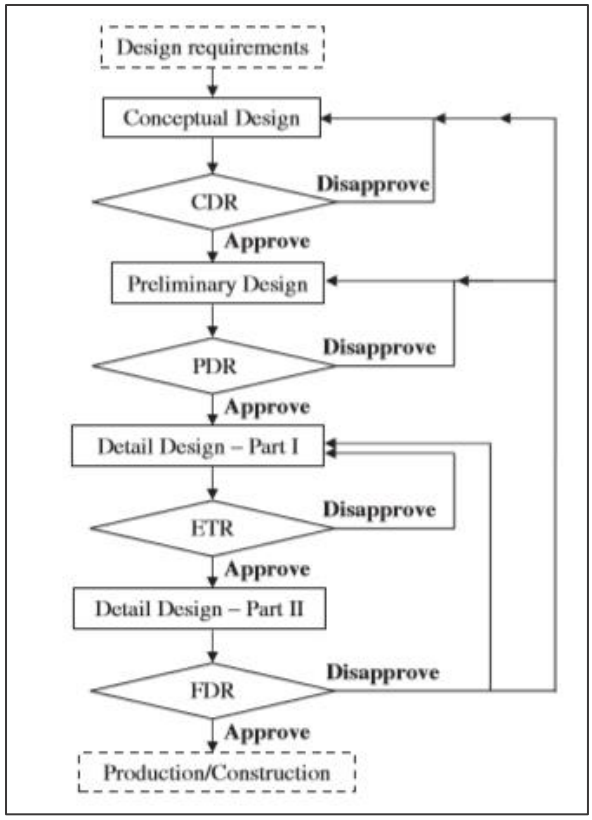

Figure 3. *Design Methodology in Aircraft Design Systems Engineering Approach, Mohammad.*

2.3 Risks consideration.

The aircraft design was made considering situations that could put aircraft in risk, decreasing the flight security. Those risks are shown in the table below:

Risk factors in the aircraft.

Risk factor	**Risk level**	**Impact**	**Mitigation method**
Strong winds	medium	High	Assure static and dynamic stability. Implementation of a gyroscope.
Telemetry failure	medium	High	Add a long range wireless connection module and physical dampers to the circuit boards to reduce vibrations
Battery discharging	Low	High	Select a battery with high amperage compared to last year
Excessive weight	High	High	Weight decreasing by using a tail boom made of composite material and reducing batteries quantity in the aircraft.
Construction delays	High	High	Better organization and improvement of the work schedule.

3 Environment Considerations

The team collected data from historical atmospheric conditions and obtained an average temperature, pressure and density prediction for Van Nuys and Ciudad Juárez. The Reynolds number was obtained using the parameters on *Table 2* with a speed of 59 ft/s as critical flight condition.

Table 2. *Parameters used to determine Reynolds number.*

	h (ft)	μ (slug/ft.s)	V (ft/s)	T (R)	ρ (slug/ft3)	P (psi)	Re
Sea Level	0	3.74E-07	59	518.67	0.002377	14.7	591,489.70
Van Nuys	711.9	3.79E-07	59	527.67	0.002326	14.33	499,732.14
Juárez	3717	3.80E-07	59	529.47	0.002134	14.65	479,071.46

To calculate Reynolds number, a spreadsheet was created, and it was calculated by using *equation 1*. Where V is velocity, l is the distance to the leading edge, ρ is density and μ is the absolute viscosity coefficient.

$$RN = \frac{\rho V l}{\mu} \tag{1}$$

The μ was calculated by *equation 2* [3], where S is the Sutherland constant, T is temperature, T_o the temperature at sea level, and μ_o the absolute viscosity coefficient at sea level.

$$\frac{\mu}{\mu_0} = \left(\frac{T}{T_0}\right)^{3/2} \left(\frac{T_0+S}{T+s}\right) \tag{2}$$

4. Overall Design Layout

4.1 Propulsion System.

The tractor configuration was selected due to the simplicity in locating the CG of the aircraft. When loading the aircraft at the front, the location of the center of mass nears the desired center of gravity, an important factor that must be considered to fly with a higher amount of payload. A tractor configuration gives more stability than a pusher configuration. Another important factor is that the engine has a more effective cooling in the front [2].

4.1.1 Engine and Propeller Selection

The engine was selected considering torque and power. Torque and power work together, but if torque fails, the airplane could lose lift, even if the engine has a lot of power, so the team opted for an engine balanced between these two factors. The *Novarossi R46F Pylon* engine was selected because of its outstanding features. As can be seen in *Table 3*, this engine was the most powerful and presented more RPM, after an empirical analysis the team found a difference on the propeller thrust of around 1.8 lb between the *Novarossi engine* and the OS 46AXII engine, being this the one of the highest efficiency.

Table 3. Engine features comparison.

Model	Power hp	RPM	Torque (lb*ft)
OS 46AXII ABL	1.63	16000	0.056
Novarossi R46F Pylon	2	33900	0.032
ASP 46A	1.3	17000	0.057

To compare propellers, the following graph was created (*Figure 4*), where the available thrust for every propeller and the thrust needed by the aircraft can be seen. The necessary thrust was calculated with the weight, density, Cl and Cd as shown in Mirandas´ book [17]. Available thrust was calculated with absorbed and output power given by Propeller Selector, a program that provides the characteristics of propulsion with a certain propeller at a specific velocity. For the RPM input, the team used values that were obtained experimentally by analyzing the Novarossi R46F engine with a tachometer.

The selected propeller was 12X6. It was found by experimental analysis, that this propeller would give more power than the other two. It was observed that the 14X6 propeller was overstressing the engine because of its torque and the 11X6 propeller had more RPMs, but the power was not as high as in the 12X6 propeller.

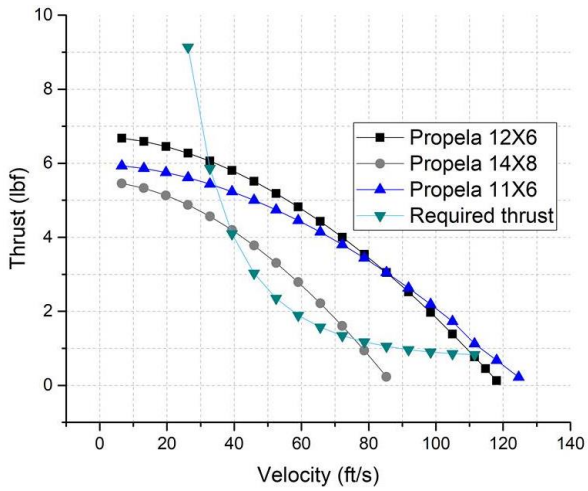

Figure 4. Comparison of different propellers

4.2 Wing Configuration and Size

The team selected a monoplane configuration for the conceptual design, this configuration is 5% to 10% more efficient than the biplane configuration. The latter would also result in a higher weight, decreasing payload capabilities. A high-wing was selected, as it satisfies the design requirements, as well as providing numerous advantages which are listed below. In *Table 3*, different configurations are compared showing their advantages and disadvantages.

Table 4. Wing vertical location: Advantages and disadvantages.

Wing vertical location	Advantage	Disadvantage
High-Wing	Facilitates unloading of dynamic payloads Easier to control Laterally more stable Higher CLmax	Increases drag 20% Heavier than low wing
Low-Wing	Less downwash on the tail Longitudinally stabilizing	Less lift High stall speed
Mid-Wing	More attractive Less interference drag	The structure is heavier More expensive

4.2.1 Wing Surface

As this year's aircraft is an optimization of the aircraft used last year, the team decided to use the same wing load of 2.88 lb/ft^2. This wing load accomplished the expected results on the previous aircraft and it was selected from a database of available technical documents about similar aircrafts from previous competitions and iterated data.

Table 5. Wing loading database.

University	Weight (lb)	Surface (ft^2)	Wing Load
University of Maryland	27.5	7.04	3.90

Polytechnic Institute of NY	55	12.77	4.30
Ecole Polytechnique de Montreal	43.24	15	2.88
Northern Arizona University	22.8	7.82	2.91
Florida International University	32.83	11.16	2.94
Old Dominion University	25.43	11.09	2.29

The aerodynamics team calculated the wing surface using *equation 3* [1].

$$S = \frac{Wto}{\frac{W}{S}} = \frac{Maximum\ takeoff\ weight}{Wing\ loading} \tag{3}$$

Where Wto is the maximum takeoff weight, in this case of 55lbs, to achieve the design objectives of have the highest possible payload, and W/S is the mentioned wing load of 2.88 lb/ft^2. This resulted in a wing surface of 2749.99 in^2.

4.2.2 Airfoil Selection

To select the most appropriate airfoil, a margin of Cl_{max} (m*aximum lift coefficient*) and Cl_i (i*deal lift coefficient*) was calculated for the wing surface of 2749.99 in^2, taking also into account the density and an approximate minimum and maximum airspeed. This margin was from 1.7 to 1.9. Initially, based on these conditions, the team selected the airfoil MH113 because it has a Cl_{max} of 1.847 at 500,000 Reynolds and its shape makes it easy to manufacture, but after analyzing the final wing with this selected airfoil and comparing that same wing with the MH114 airfoil (which was used in the past competition), it was observed that the MH114 was 5% more efficient with a minimum difference in the Cl_{max}, which was 0.031 less than the MH113 airfoil. Due to this advantage, it was decided to keep last year's airfoil instead. The comparison between the wing efficiency with the two different airfoils is shown below in the right side of *Figure 5* and the difference between the airfoils' lift coefficient is shown in the left side of the figure.

Table 6. Different airfoils features.

Airfoil	**Cl_{max}**	**α_s**	**Cd_{min}**	**α_{Cdmin}**	**Cl_0**	**α_0**	**Cm_0**	**$(Cl/Cd)_{max}$**	**$\alpha_{(cl/cd)max}$**	**Cl_{Cdmin}**	**Cd_0**
EPPLER 423	2.038	12	0.011	-2	1.114	-11	-0.239	133.124	5	0.8912	0.011
MH 112	1.856	15	0.009	0	0.927	-15	-0.200	129.293	5	0.9267	0.009
MH113	1.847	15	0.009	1	0.892	-12	-0.194	135.040	3	0.9994	0.009
MH 114	1.816	15	0.008	0	0.877	-11	-0.195	140.593	4	0.877	0.008

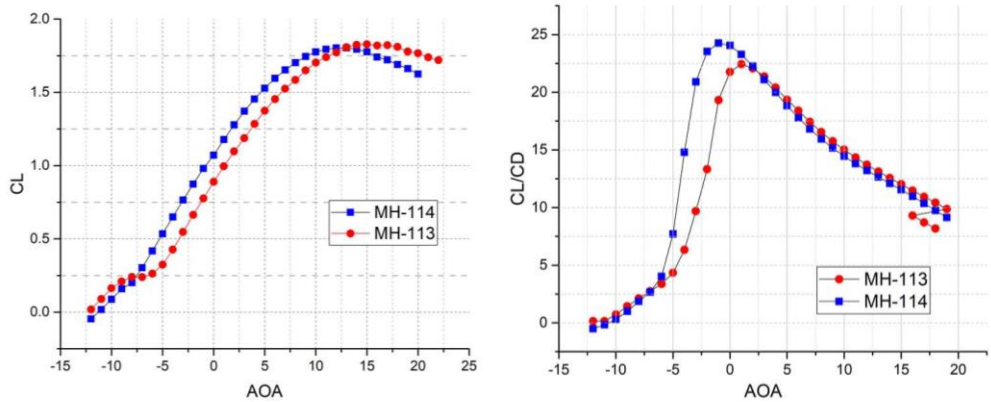

Figure 5 Comparison between the MH114 and MH113 airfoils: Cl vs AOA airfoil and CL/CD vs AOA of a wing with different airfoil.

4.2.3 Aspect Ratio

The selection of the AR was made through an iterative process, starting with a literature research in which high and low ARs were compared. It was then decided to use a high AR wing due its efficiency. Aspect Ratios of 7, 8 and 9 were compared between their CL_{max} and CL/CD. The AR of 9 resulted in higher efficiency and lift but increased wing deflection so was discarded. Then the same comparison was made but now with a more specific range of AR, from 7.8 to 8.2. From results obtained in the XFLR5 software, an AR of 8 was selected having a CL_{max} of 1.692.

4.2.4 Wing Planform

Different wing planforms were analyzed, such as rectangular, tapered, mixed wing and elliptical wing. After choosing the airfoil, surface area and AR, the planforms were evaluated in a decision matrix and compared in their aerodynamic characteristics, cost and manufacturing simplicity. The rectangular and tapered wing planforms were selected since they met the team requirements. These were analyzed using XFLR5 as well as through mathematical methods. The planform selected was a tapered wing with a taper ratio of 0.8, as shown in F*igure 6*, as it is more efficient than a rectangular wing with the same AR and wing surface and it fulfills the team objective to have a good lift performance to accomplish the mission.

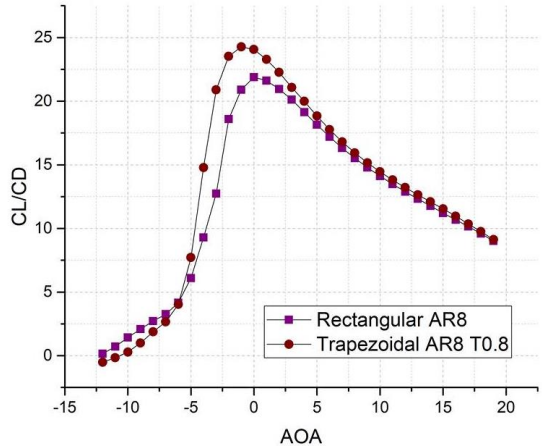

Figure 6 Comparison between tapered and rectangular wing.

4.3 Vehicle Configuration Selection

For the landing gear configuration, a nose gear was selected over taildragger because the taildragger requires a high skill in flying for the landing stage of flight. A conventional landing gear was determined to be the best configuration for the easiest operation of the aircraft during taxi, landing and take-off.

4.4 Competitive Scoring and Strategy Analysis

According to the design implemented and the characteristics of the conceptual design, such as maximum static payload and number of dynamic loads, it was estimated that a score of around 200 points could be obtained for the aircraft's flight rounds performance. *Figure 7* shows the scoring equation which the team was based on to make estimates of an approximate score. For these estimates, the team considered only two releasable payloads and an ideal scoring prediction.

Scoring Equation:

$$FFS = Final\ Flight\ Score = 4 \times \left(\frac{1}{N}\sum_{1}^{N} FS\right)$$

Where:

$$FS = Flight\ Score = S_p + \left(S_p \times \sum Z_m\right)$$

Z_m = Zone Multiplier

S_p = Static Payload (lbs)

N = Total Number of Flight Rounds During Competition

Round	Sp (*lbs*)	∑Zm /round	FS
1	20	1.5	50
2	20	1.5	50
3	20	1.5	50
4	20	1.5	50
5	20	1.5	50
6	20	1.5	50
		FSS	200

Figure 7 SAE scoring equation (left) and the team's scoring assumption (right).

4.5 Optimization

Because the design of the current aircraft(*EURUS*) is an optimization of the last years 'aircraft, certain features were analyzed to make relevant improvements. The overall wing design of the *2017 aircraft* (*EHECATL*) consisted in a rectangular geometry with an AR of 7.5 and a surface of 15.625$ft2$, to improve its performance was opted increase the aerodynamic efficiency increasing the surface and AR, as well as a conicity of 0.8 was added to decrease drag and by this way achieve the goal of an aircraft with high aerodynamic performance with a maximum take-off weight of 55 lbs. The *EURUS* lift wing was increased by 32% compared to the *EHECATL wing* with a decreased in drag of -3.5%. The *figure 8* shows the efficiency increase on the aerodynamics conditions of the wing.

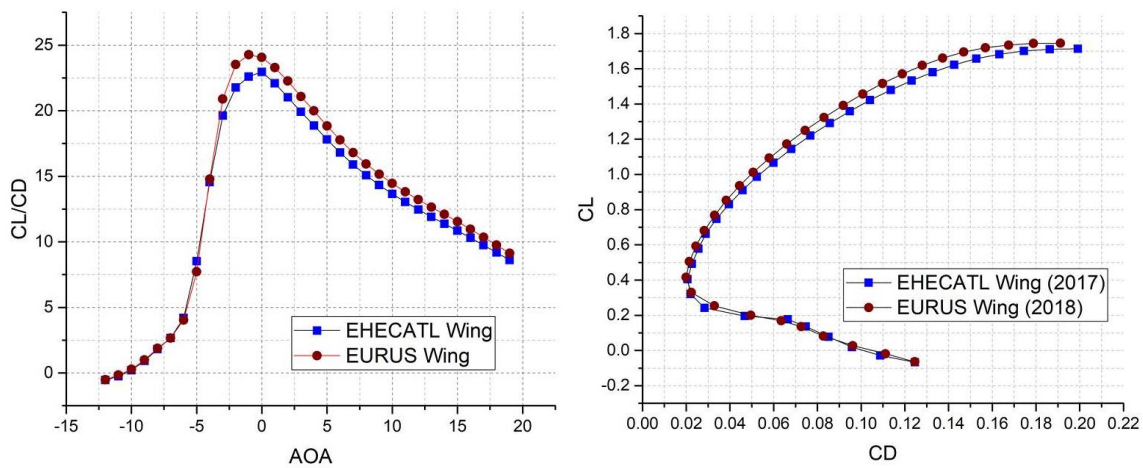

Figure 8. Efficiency comparison between last year´s model and present model.

5 Analysis

5.1 Analytical Tools (CAD, FEM, CFD, etc.)

The team used ANSYS and ANSYS APDL as a software tool to perform the finite-element analysis, as well as software such as XFLR5 and Propeller Selector, which were used to make the comparisons between different airfoils and wing configurations, and the analysis to propeller selection.

5.2 Performance Analysis

5.2.1 Static and Dynamic Thrust

To calculate static thrust, the team used equations 4 and 5:

(4) (5)

$$T_{v=0} = K_{T0} \cdot \frac{P_E}{n \cdot D} \qquad K_{T0} = 57{,}000 \cdot (1.97 - \frac{P}{D})$$

K_{T0}= 87, 721.03; $T_{V=0}$=7.63 lbf

Regarding dynamic thrust, the available thrust decreases as velocity increases, and the required thrust decreases. RPM were found by experimental analysis: we put the engine in a testing bench and measured with a tachometer the corresponding RPM for each propeller.

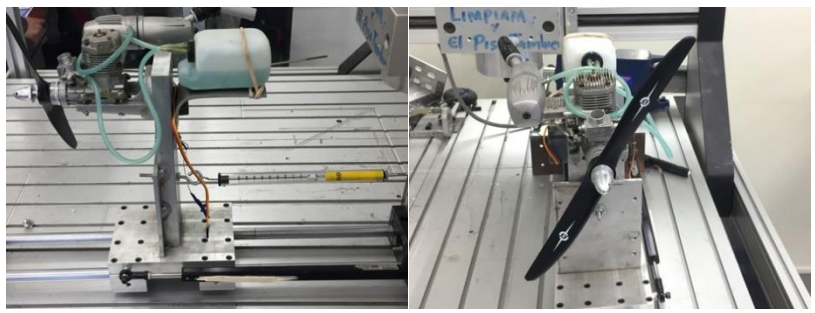

Image 1. OS engine mounted on the testing bench.

5.2.2 Take-off and Landing Performance

The take-off distance is represented here according to weight and takeoff velocity. For the take-off analysis, it is necessary to use Newton´s Second Law of motion. Several factors are involved in calculating it, such as weight, Cl, S and density. The method used for the take-off analysis is shown by the author Miranda [17]. The FAA recommends that the take-off speed should be 20% greater than the stall speed. In the following figure, the take-off and landing distance are shown, as well as approach velocity according to weight. The equations used for the drag and lift are the same used for take-off and an approximate measure of the competition runway was taken as basis for calculating distances.

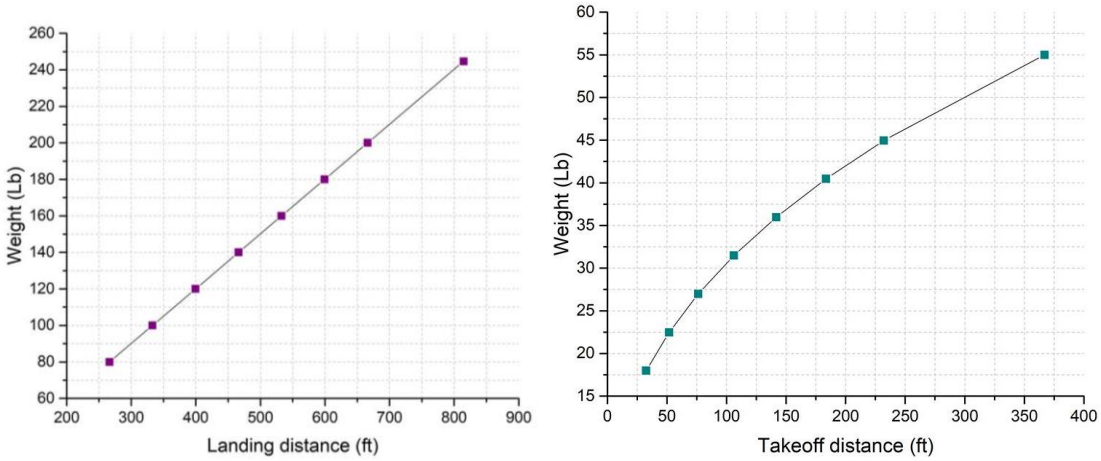

Figure 9. Landing and Take-off distances.

5.2.3 V-N diagram

The V-N diagram was made to find the structural limitations of the aircraft. The maximum load factor (which is defined as lift/weight) as established by the team was 2.5. It was found that for this type of aircraft the recommended maximum load factor is 2.5, and if this factor is exceeded, the aircraft will risk structural integrity, so there is a limited load factor which is dependent on speed. *Figure 10* shows this relationship so that it may be studied for any speed and the maximum load factor may be established for it. A load factor above 2.5 may put the aircraft at risk, and if anything above an upper limit of 3.75 is exceeded, the aircraft will surely lose structural stability and integrity.

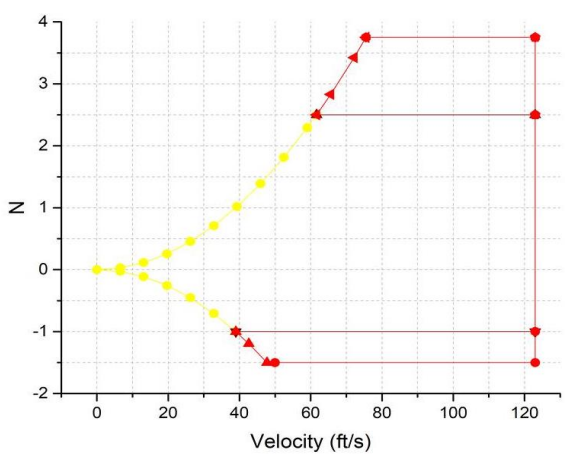

Figure 10. V-N diagram.

5.2.4 Payload Prediction

The maximum load that can be applied to the aircraft if it is to be operated at a certain height is shown below. It is calculated taking the thrust capacity of the engine. Take-off estimates were used for every

density. The goal was to maintain constant take-off distance for every density, so that limitation determined how much payload the aircraft could carry.

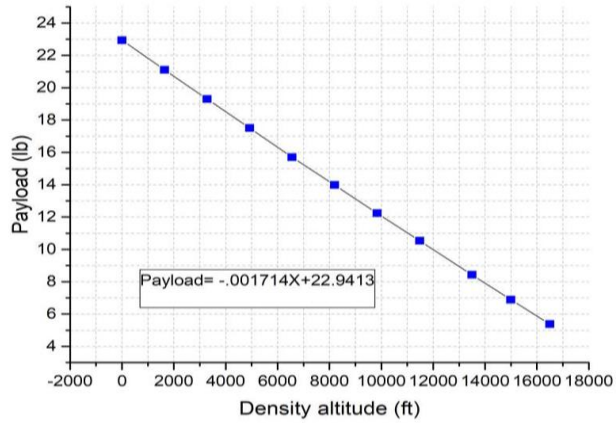

Figure 11 Payload prediction graphic.

5.2.5 Flight Performance.

The team based on Raymer's method [16] and Nicolai´s method [6] to estimate the Drag polar as shown in *figure 12* to compare the different results. A CD_0 of 0.0116 was obtained through the analytical analysis similar as that obtained through CFD analysis which was around 0.0112.

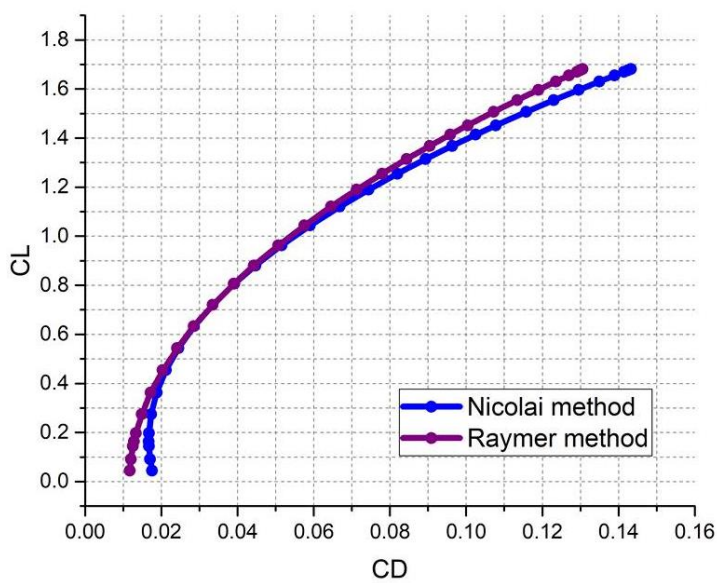

Figure 12 Payload prediction graphic

5.2.6 Maneuver Performance

The graph below shows the load factor that the aircraft experiences when making a turn maneuver at a certain velocity. As calculated, the approximate angle at which the aircraft will make turns is 44

degrees. This is very important because it represents a load factor, and it needs to be ensured to not exceed 2.5 to avoid risking the structure. Turns for maneuvering will be made with an approximate radius of 9.7 ft.

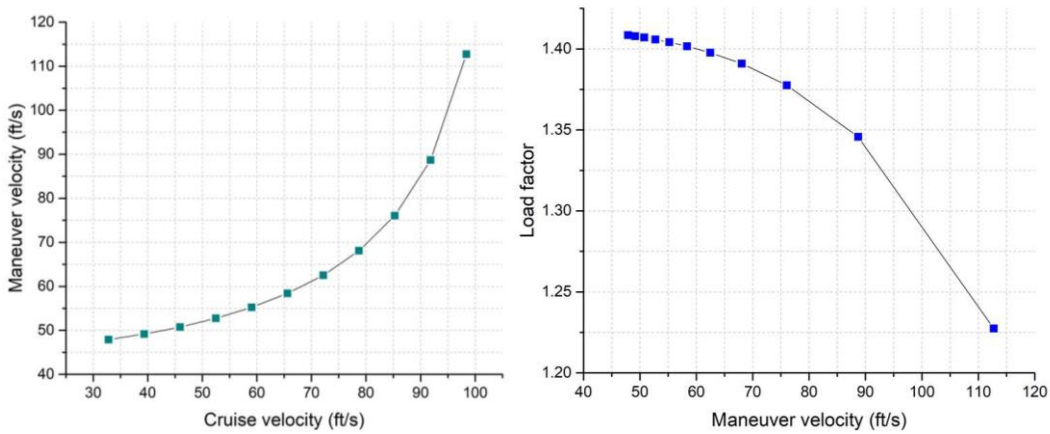

Figure 13. Load factor analysis on maneuver velocity.

5.2.7 Dynamic & Static Stability

As the main purpose of the Advanced category is to accurately drop a dynamic payload, the aircraft must have a good stability and control to maintain the desired altitude and flight path, overcoming any disturbance. Following an iterative methodology, the horizontal stabilizer volume was varied (V_H) within the range of 0.3 to 0.6, and 0.02 to 0.05 for the vertical stabilizer volume coefficient (V_V), and the moment arm for each stabilizer in the formulas 6 and 7:

$$V_H = \frac{S_H l_H}{Sc} \quad (6) \qquad V_V = \frac{S_V l_V}{Sc} \quad (7)$$

The aircraft stability depends mainly on the position of the center of gravity (CG) with respect to the neutral point (NP) and the tail sizing. Longitudinal stability is archived when the aircraft total variation of pitching moment versus angle of attack (Cmα) is negative and the CG is forward of the NP. Cmα was calculated considering the contribution of three main components: wing, tail, and fuselage, as seen in the following table.

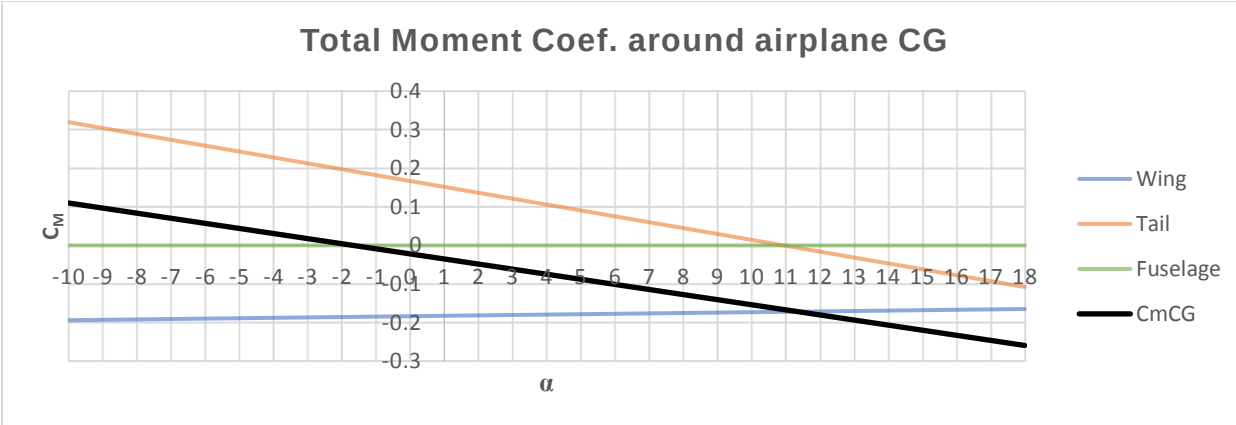

Figure 14. Total moment coefficient around the aircraft's CG graph.

For directional static stability, Cn_β must be positive. This stability derivative was evaluated for wing/fuselage and vertical tail contribution. Finally, the requirement for lateral static stability, is that Cl_β must be negative, and since the wing is non-swept, for its analysis it was only considered: dihedral effect, wing vertical position and vertical tail contribution.

Table 7. Static stability derivatives

Derivative	Value
Cmα	-0.8148
Cl_β	-0.1146
Cn_β	0.0626

To evaluate the dynamic stability of the aircraft, an engine mode analysis was performed for both longitudinal and lateral-directional stability for fully loaded case. The main parameter of each mode can be seen in *Table 8.*

Table 8. Level 1 Stability Requirements and principal mode parameters

Mode	Level 1 Requirement	Loaded Case	Stability Level
Phugoid	ζ > 0.04	ζ = 0.041	Level 1
Short Period	0.35 < ζ < 1.3	ζ = 0.616	Level 1
Roll	τ < 1 s	τ = 0.033	Level 1
Dutch Roll	ζ > 0.08	ζ = 0.179	Level 1
	ω > 0.4 rad/s	ω = 3.701 rad/s	
	ζω > 0.15 rad/s	ζω = 1.733 rad/s	
Spiral	Tdouble > 20 s	Tdouble = 9.413 s	Level 2

The team's goal was to get “Level One Stable” defined as “excellent aircraft characteristics” and “pilot compensation not a factor” [8] in each stability mode. Spiral stability did not meet level 1 requirements,

which is common, but level flight can be compensated by pilot input. As an experienced pilot is not ensured, it was decided to implement a gyroscope to maintain stability.

Based on the 2017 competition, the team followed the recommendations for control surface sizing from reference (5) and (1). The torque needed for each control surface was calculated in function of the mean chord of the control surface ©, the length of the control surface (L), the speed (V), the maximum surface deflection, and the maximum deflection of the servo.

$$\boldsymbol{\tau = 8.5x10^{-6}\ \frac{C^2V^2L\ sin(S1)\tan(S1)}{\tan(S2)}} \tag{8}$$

The necessary torque and the sum of control surfaces' dimensions are showed in *Table 9*. To avoid overloading the servos, they were selected with a 1.5 safety factor.

Table 9. Necessary torque and summary of control surfaces dimensions

Control Surface	**Surface recommendation (%)**	**Surface (in^2)**	**Torque (ozIn)**
Aileron	3.0-12	275 (10%)	60.713
Rudder	15-35	158.27 (35%)	25.467
Elevator	15-40	102.453 (30%)	42.433

5.2.8 Telemetry system

The DAS system implemented an AltiMU-10-v5 barometric sensor, an Arduino Nano as microcontroller, and a Xbee 900HP for wireless connectivity. The Arduino was programmed to read the barometric pressure from the sensor and calculate the altitude and send the data through the Xbee. When the aircraft is powered on, the Arduino first gather data to calculate the local atmospheric conditions and set the ground elevation, from which the altitude is measure. Also, the Arduino is also programmed to release the dynamic payloads when the command is given.

The past figure shows the block diagram for the aircraft telemetry system. As shown, a FPV system is also implemented as the rules required it. Last year, the main problem was the loss of connectivity between the aircraft and the ground station. For this competition, the use of the same frequency for the DAS and the radio control was not allow to avoid interference, which was a reason for last year malfunction.

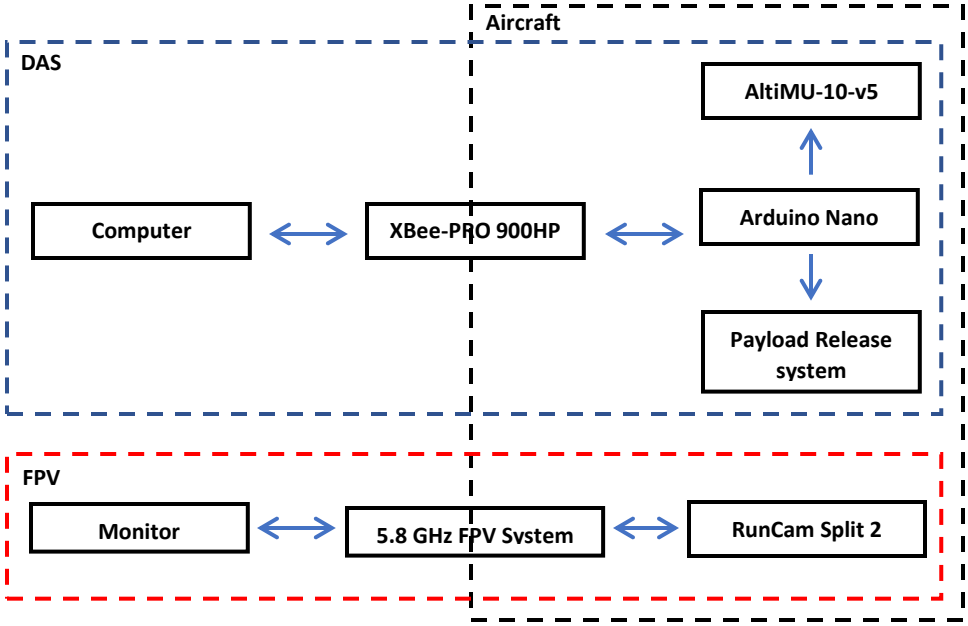

Figure 15. Telemetry block diagram

5.3 Structural Analysis

5.3.1 Spar analysis

A Security factor of 1.4 was selected for this type of aircraft. This factor is intended to cover some possible uncertainties in loads, variations in the manufacture of components and discrepancy in strength properties of materials. With a lift force resultant from each half of the wing of 31.02lbf, applying the security factor we obtained an ultimate load of 43.43017 lbf.

A cross-section of ¼ x 1 in was selected giving a moment of inertia of $.02083in^4$ and the centroid is at 0.5in from the base.

Analyzing the spar as a cantilever beam we could get the maximum bending moment and therefore obtained the resultant maximum normal stress in the spar.

$$\sigma max = \frac{1650.20lb * in * .5in}{.2083in^4} = 3961.113\frac{lb}{in^2} \tag{9}$$

With these results we considered using Al 6061 T6 with the previously mentioned cross-section area because it has a yield tensile stress of 40 psi.

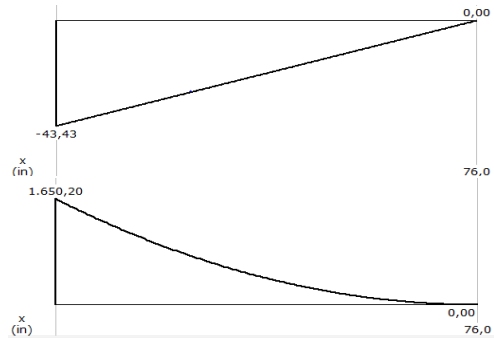

Figure 16. Shear force(top) and Bending moment diagrams (bottom)

5.3.2 Mass Properties & Balance

The team analyzed different materials to select the optimal option that improve the aircrafts design, balsa wood, AL6061 and AL2024 was The selection of strong, lightweight materials for the aircraft is very important, because it is a limiting factor in how much weight can be carried. The material selected also dictates how much the aircraft

Table 10. Materials properties.

Material	Density (*lb/in³*)	Yield Strength (*Ksi*)	Elastic Modulus (*Ksi*)	Poisson's Ratio
Balsa wood	0.00324	1.015	538	0.38
AL6061 T6	0.0975	40	10000	0.33
AL2024	0.1	47	10600	0.33
Carbon fiber	.0813	8.99	1600	.17

To do the weight and balance analysis, the center of mass and the weight of each component was consulted in the manufacturer datasheet. Its location was estimated using SolidWorks computer- assisted modeling. *Table 11* shows the weight and moment of all components according to their position.

Table 11. Weight and balance analysis.

Component	Weight (lb)	Arm (in)	Momentum (lb in)	Component	Weight (lb)	Arm (in)	Momentum (lb in)
Avionics	0.1979349	32	6.3339168	Nose gear	0.2606156	6.35	1.65490906
Battery	0.68	4.3	2.924	Propeller	0.124375	-4.31	-0.53605625
FPV Camera	0.317466	12	3.809592	Voltage regulator	0.0551156	14	0.7716184
Fuel Tank	0.375	14.5	5.4375	Receiver	0.044092452	14	0.617294334
Empennage	1.1	84	92.4	Servos Empennage	0.226	83	18.758
Engine	0.910509	-3.45	-3.14125605	Throttle Servo	0.113	2.6	0.2938
Tuned pipe	0.175	7.5	1.3125	Spinner	0.0308647	-4.5	-0.13889115
Tailboom	0.75	59	44.25	FPV Transmitter	0.0685017	12	0.8220204
Fuselage	1.15	27	31.05	Wing	7.5	20	150
Main landing gear	0.6337757	29.13	18.46188614		Total W.	Total M.	C.G. Arm
Engine Mount	0.56	-2	-1.12		**15.2722507**	**373.9608**	**23.13**

6. Aircraft ‘s assembly.

The aircraft contains three main assemblies: the wing-fuselage union, the tail boom to fuselage union and the tail to tail boom union. The first one is shown on *image 2*, it was made of Aluminum 6061 T6 to support the long wing momentum. The tail boom assembly to the fuselage and tail was made of 1/8 plywood.

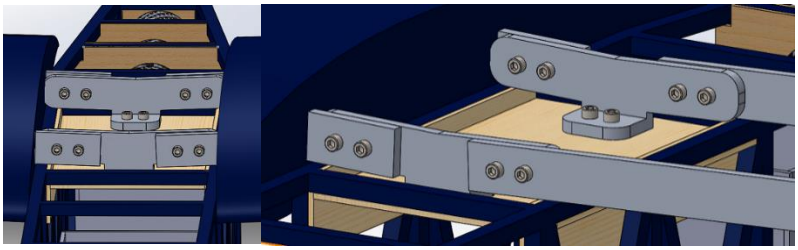

Image 2. Wing support assembly.

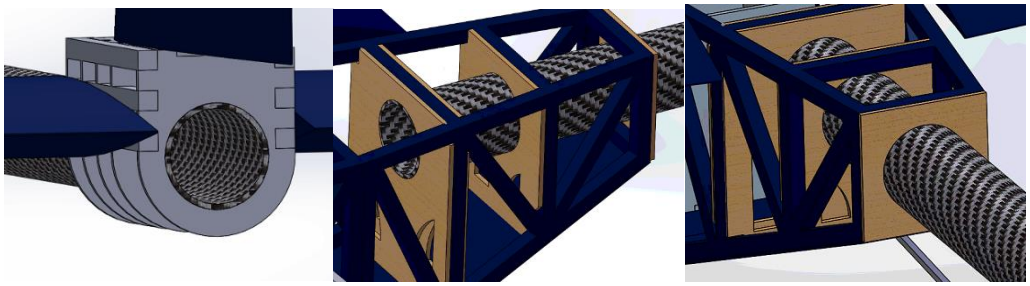

Image 3. Tail boom to fuselage and tail assembly.

7. Manufacturing process

To manufacture the main structure of the aircraft, the team was based on the design drawing that is shown on *image 4*, which was used as a guide to build the truss structure composed of diagonal and vertical members, as well as crossbars of balsa wood of 3/8in x 3/8in. In *Image 4*, the construction of the truss structure and the design drawing used are displayed.

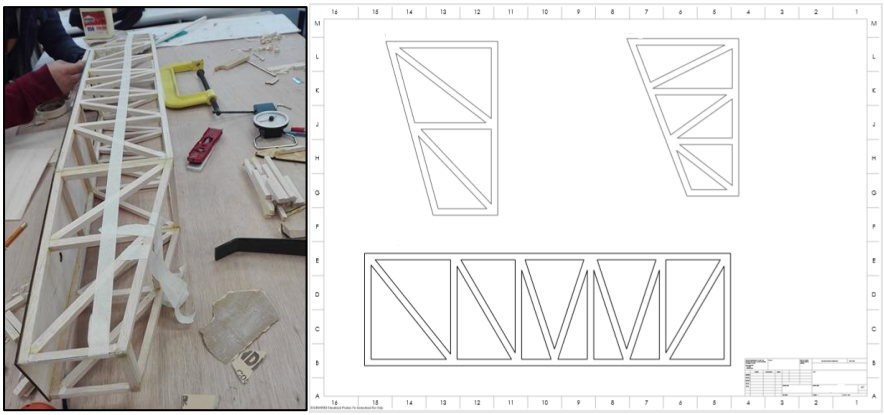

Image 4. Airframe construction and design drawing.

To optimize construction time and accuracy, the ribs of the wing and the empennage were cut by laser. *Image 5* shows the cutting process and the final product of the cut of two of the wing ribs, respectively.

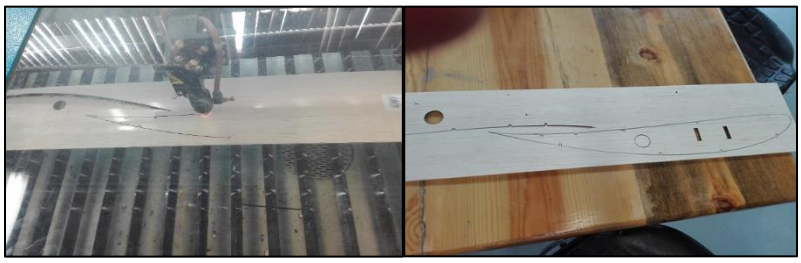

Image 5. Ribs cutting process and wing ribs final cut.

Since the distances between the ribs needed to remain as in the design, the spacing in the main spar was carefully measured with the help of a Vernier and each rib was positioned in its proper place as can be observed in the following images.

Image 6. Ribs arrangement.

The components to maintain the wing position and dihedral angle (*wing supports*), were worked on with a CHEVALIER QP1620-l machining center. The G-code for the machine was done in the *Featurecam* software and the team made the necessary corrections of any errors caused by the software to have a successful process. The machining time was approximately of 3 hours for each component.

Image 7. CNC machining of wing support.

8. *Cost analysis*

The project´s cost analysis is shown on the following table.

Manufacturing materials		Cost USD	Quantity	Total USD
Balsa wood		$11-$32	284	$400.00
Plywood		$5.25	4	$55.00
Adhesives		$1.75 - $25	50	$323.56
Monokote/Ultracote		$12	12	$144.00
Screws and Bolts		$20		$20.00
Miscellaneous			**Subtotal**	$437.33
Aircraft Parts				
Motor		$200	1	$200.00
Spinner		$5.05	1	$5.05
Propeller		$10	3	$30.00
Engine Mounts		$30	1	$30.00
Nose Landing gear		$15.95	2	$31.90
Wheels		$1.11	6	$6.66
Collars		$2.19	4	$8.76
Wheel Axle		$1.49	6	$4.47
Main Landing Gear		$27	2	$54.00
			Subtotal	$370.84
Electronics				
LiPo Batteries		$41	2	$82.00
NiMH Batteries		$7.46	2	$14.92
Control Battery		$9.99	2	$9.99
Wire and Connectors		$8.96	3	$26.88
Servo motors		$15.65	7	$109.55
			Subtotal	$243.34
			Total	$1,051.51

9. Conclusion

As mentioned, the design of the present aircraft is an optimization of last year's aircraft, the team focused in improving stability, structure strength, telemetry and propulsion characteristics. A selection criterion was made in which all the good things of last year´s aircraft were taken and making a visualization of what could improve in this new one, we developed an iterative process to finish design.

The characteristics and design in this aircraft assures that the aircraft will have a stable flight in the conditions of the competition dropping the loads accurately and flying safe according to all of the competition´s rules.

APPENDIX B

Advanced Class Tech-Data Sheet: Radio Link Budget

Supply data for each transmitter used onboard the aircraft. Expand number of columns as needed. Calculations for Radio control systems using 2.4GHz are optional.

Radio System Function (FPV, DAS, RC, Payload)	Units	FPV	DAS	RC	Payload Release
Operating Frequency (F)	MHz	5800	900	2400	900
Wavelength (WL) = 300 / F Hz)	meters	0.0517	0.3333	0.125	0.3333
Maximum Operating Range (Rng)	meters	5000	6500	1608	6500
Free Space Path Loss (Lfs) = 20Log(4Pi (Rng / WL))	dB	121.6937	107.784	104.171	107.784
Transmitter Brand & Model ID		Boscam TS832	Digi XBee-PRO 900HP	Turnigy TGY-i10	Digi XBee-PRO 900HP
Transmitter FCC ID	FCC ID	NA	MCQ-XB900HP	N4ZTGYI10	MCQ-XB900HP
Transmitter Power (Pt)	dBm	27.5	24	20	24
Number of Transmitter Channels Available	---	40	63	10	63
Transmit Antenna Gain (Gt)	dB	5	2.1	2	2.1
Transmit Antenna Polarization	H, V RHC, LHC	RHC	V	V	V
Transmit Line or Misc. Losses (Lt)	dB	0	0	0	0
Receive Line or Misc. Losses (Lr)	dB	0	0	0	0
Receive Antenna Gain (Gr)	dB	14	2.1	0	2.1
Receive Antenna Polarization	H, V RHC, LHC	V	V	V	V
Polarization Mismatch Loss (Lpol)	dB	3	0	0	0
Power Rcvd (Pr) = Pt + Gt + Gr – Lfs – Lt – Lr – Lpol	dBm	-78.19	-79.584	-82.171	-79.584
Receiver Signal Power Required (Pmin)	dBm	-90	-82.334	-105	-82.334
Signal Margin = Pr – Pmin	dB	11.81	2.75	22.829	2.75

FPV Transmitter Operating Frequencies Available (MHz).
If your video transmitter or data-link operates on a frequency which can be changed, list all the available frequencies below and highlight the one you intend to use. If your system is spread spectrum, list the range of frequencies you intend to use.

5865	5845	5825	5805	5785	5765	5745	5725
5733	5752	5771	5790	5809	5828	5847	5866
5705	5685	5665	5645	5885	5905	5925	5945
5740	5760	5780	5800	5820	5840	5860	5880

10 References

[1] Sadraey, M. H. (2013). Aircraft design: a system engineering approach. Wiley.

[2] Anderson Jr., J. (1999), Aircraft Performance and Design. McGraw-Hill.

[3] Carmona, A. I. (2002), Aerodinámica y actuaciones del avión.

[4] Abbot, I.H., & Von Doenhoff, A.E. (1959), Theory of Wing Sections. Including a Summary of Airfoil Data.

E.U.A. Elsevier, Inc.

[5] Etkin, B., & Reid, L. D. (1996). Dynamics of flight: stability and control. Wiley.

[6] Nicolai, Leland M. (2009). Estimating r/c model aerodynamics and performance.

[7] Simons, M. (1994). Model aircraft aerodynamics. Argus Books.

[8] (1980). MIL-F-8785C Military specification flying qualities of piloted airplanes.

[9] Results - SAE Aero Design. (n.d.). Retrieved August 22, 2016, from

http://students.sae.org/cds/aerodesign/results/

[10] Faludi, R. (2011). Building wireless sensor networks. O'Reilly.

[11] Wood handbook: wood as an engineering material. (1974). Madison: The Laboratory.

[12] Florida International University. (2015). 2015 SAE Aero Design East Competition. Retrieved from

www.eng.fiu.edu/mme/robotics/EML4551SeniorDesignOrg/Presentation/2014Fall/Team18FinalPresentation.ppt

[13] Northern Arizona University. (2013). SAE AERODESIGN WEST “THE WRIGHT STUFF”. Retrieved from

https://www.cefns.nau.edu/capstone/projects/ME/2013/TheWrightStuff/images/UGRADSReport.pdf

[14] Old Dominion University. (2015). 2015 SAE Aero Design East Technology Report. Retrieved from

http://dasp.mem.odu.edu:8080/~aero_sp15/TechReport.pdf

[15] Polytechnic Institute of NYU. (2012). SAE Aero Design Report 2012. Retrieved from

http://edge.rit.edu/edge/P16121/public/Benchmarking/Reports/Sae%20Aero%20Design%20West%20Report,%20Polytechnic%20Institute%20of%20NYU,%20213.pdf

[16] Raymer, D.P. (2004). *Aircraft design: A conceptual approach.* Retrieved from

http://soaneemrana.org/onewebmedia/AIRCRAFT%20DESIGN%20%3B%20A%20Conceptual%20Approach%20BY%20DANIEL%20P%20RAYMER.pdf

[17] Miranda L.E. (2013), *Fundamentos Da Engenharia Aeronáutica*.PDF